 doi:10.20944/preprints202211.0132.v1

*Article*

# Natural products as Potential Inhibitors of APH(3')-IIIa of *Enterococcus faecalis*: An *In-silico* Perspective

**Juan Marcelo Carpio Arévalo[1] and Juliana Carolina Amorim[1*]**

[1] Academic Unit of Health and Wellness, Catholic University of Cuenca, Cuenca, Azuay, Ecuador; juanbiomarce@gmail.com

*Corresponding author: julianacarolinaamorim@gmail.com

**Abstract:** *Enterococcus faecalis* is a bacterium that can develop a multidrug resistance profile associated with the community as well as nosocomial-acquired infections. Among the treatment options for these infections are aminoglycosides combined with bacterial cell wall inhibitors such as beta-lactams, since *E. faecalis* is intrinsically resistant to aminoglycosides. One of its most representative resistance mechanisms is the expression of aminoglycoside-modifying enzymes, such as the aminoglycoside phosphotransferase type IIIa of *E. faecalis* (*Ef*APH(3')-IIIa). This enzyme acts by phosphorylating aminoglycosides in an ATP-dependent reaction, modifying the 3' position of hydroxyl groups of these antibiotics. Considering this scenario, 3,092 natural products obtained from the ZINC22 database were analyzed to select molecules with the highest affinity for the nucleotide-binding pocket of *Ef*APH(3')-IIIa, which could be potential aminoglycoside adjuvants. The molecules that showed the best-score results obtained from ensemble docking-based virtual screening were ZINC000000952700 (BS-1), ZINC000014793040 (BS-2) and ZINC000015498603 (BS-3). The most promising results were for BS-2, a flavone derivative, due to its improved stability profile in molecular dynamics simulation (average values of RMSD of 0.23 nm, and Rg of 1.94 nm), binding free energy calculations (average ΔG total of -35.3 nm), as well as better toxicological profile (lower probability of hepatotoxicity, carcinogenic, immunotoxicity, mutagenicity, and cytotoxicity effects), compared to BS-1 and BS-3. These results allow us to propose that a flavone derivative may act as an adjuvant to aminoglycosides in the treatment of *E. faecalis* infections, acting as an inhibitor in the nucleotide-binding pocket of *Ef*APH(3')-IIIa.

**Keywords:** *Enterococcus faecalis*; natural products; aminoglycosides; aminoglycoside-modifying enzymes; APH(3')-IIIa; flavone derivative

## 1. Introduction

Antibiotics represent one of the greatest advances in modern medicine, they have been able to combat the major infectious diseases that have threatened human survival and development for more than a century of use [1,2]. However, the prolonged and often unguided use of these medicines has led to widespread resistance phenomena [3]. Among the numerous bacterial species capable of developing resistance to a broad spectrum of antibiotics is *Enterococcus faecalis* [4]. This potential gives this bacterium a selective advantage over other species that share the same environment, thus allowing it to spread further than others [4,5]. Therefore, although *E. faecalis* is part of the normal human microbiota it can become opportunistic, in this condition it is the most prevalent species of the genus Enterococcus in the total infection events, with approximately 80-90% of cases [6,7]. The most common community infections caused by this species are infective endocarditis, gastrointestinal and urinary infections [8]. On the other hand, sepsis, meningitis, and catheterization procedures, especially in intensive care settings, are some of the causes of nosocomial complications [4,5,9]. Furthermore, the high number of these conditions is due to *E. faecalis* exhibiting an intrinsic resistance to many antibiotics, among them the aminoglycosides [7,10].

 doi:10.20944/preprints202211.0132.v1

Aminoglycosides are antibiotics effective in the treatment of Gram-positive and Gram-negative bacteria [11]. One of the mechanisms of action is the inhibition of the initiation or elongation phase of bacterial protein synthesis due to binding to the 30S ribosomal subunits [12,13]. The aminoglycosides are efficient in enterococci only when used in conjunction mainly with beta-lactams, which facilitate the entry of aminoglycosides due to the impairment of the synthesis of the bacterial cell wall [5]. Among the main bacterial resistance mechanisms developed over time against aminoglycosides is the expression of aminoglycoside-modifying enzymes (AMEs) [11]. These enzymes act on the catalysis of covalent modifications in specific amino and hydroxyl groups of most of the aminoglycosides available for clinical use [11,13]. Based on these modifications, this class of antibiotics begins to bind weakly to bacterial ribosomes, reducing its efficiency. AMEs can be of three different families according to their modification mechanism [13]. *N*-acetyltransferases (AACs) are the enzymes that modify aminoglycosides using acetyl coenzyme A to modify amino groups of aminoglycosides [14]. While the enzymes responsible for using ATP to modify hydroxyl groups of aminoglycosides are *O*-nucleotidyltransferases (ANT) and *O*-phosphotransferases (APH) [12,13]. Generally, only the APH are capable of generating high levels of resistance and can phosphorylate specific hydroxyl groups of all types of aminoglycosides, so they are more widely studied [13].

The APH family is divided into seven classes, the largest of which is called APH(3'), responsible for phosphorylating hydroxyl groups of aminoglycosides at the 3' position [12,13]. This class is in turn divided into seven types called APH(3')-I to APH(3')-VII [15]. Assessments of different clinical isolates of *E. faecalis* in several countries have shown that the phenotype of resistance to aminoglycosides expressing the *aph(3')-IIIa* gene is mainly due to the extended use of amikacin, kanamycin and streptomycin [7,16–18]. Knowing a long time that research and development of new antibiotics takes, one option is to find adjuvants that can be associated with them to restore their efficacy [19]. In this context, natural products reappear as candidates of great interest for various therapeutic applications [20–24], mainly due to the broad diversity of their scaffolds [25]. Based on this need, in the present work, 3,092 natural products were selected to evaluate their potential to act as competitive inhibitors in the nucleotide-binding pocket of APH(3')-IIIa of *E.faecalis* (*Ef*APH(3')-IIIa).

## 2. Methods

*Ligands and target preparation*

The chemical structures of the 3,092 natural products were downloaded from the Biogenic Catalogue of ZINC22 [26] database in SDF format using the server Arthor [27] in May 2022. This database was filtered with DataWarrior-5.5.0 [28] to include ligands with up to 5 hydrogen bond donor groups and up to 10 hydrogen bond acceptors. Next, hydrogen atoms were assigned to the structures at pH 7.4 for all the ligands, the 3D structure was generated as default, followed by minimization steps of these structures with the MMFF94 force field [29] using the steepest descent geometry optimization with 500 steps, followed by conjugate gradient algorithm with default parameters and transformed into MOL2 format, all using Open Babel-3.1.1 software [30]

All *Ef*APH(3')-IIIa 3D x-ray diffraction structures were obtained from RCSB Protein Database (PDB ID: 2BKK, Resolution: 2.15 Å; R-Value Free: 0.260; R-Value Work: 0.199; R-Value Observed: 0.200, C-chain, co-crystallized with ADP [31]), (PDB ID: 3Q2J, Resolution: 2.15 Å; R-Value Free: 0.235; R-Value Work: 0.189; R-Value Observed: 0.194, chain B, co-crystallized with CKI-7 [32]) and (PDB ID: 3TM0, Resolution: 1.58 Å; R-Value Free: 0.204; R-Value Work: 0.176; R-Value Observed: 0.178, chain A, co-crystallized with ANP [33]). All crystals were prepared using the Dock Prep module of UCSF Chimera-1.16 [34] using default parameters, then were converted into PDBQT format using the Auto-Dock-Tools-1.5.6 [35].

Preprints (www.preprints.org) | NOT PEER-REVIEWED | Posted: 8 November 2022 doi:10.20944/preprints202211.0132.v1

*Ensemble docking-based virtual screening and molecular dynamic simulations*

The ensemble docking-based virtual screening strategy was conducted with AutoDock Vina-1.1.2 software [36] on the crystal coordinates corresponding to the nucleotide-binding pocket of 2BKK, 3Q2J and 3TM0 selected crystals. These coordinates were 10.3, 27.7 and -10.4 on the x, y and z axes of the 2BKK; 27.9, 9.6 and 70.7 on the x, y and z axes of the 3Q2J; and also 51.3, 42.5 and 15.5 on the x, y and z axes of the 3TM0. And all box dimensions were 30 x 30 x 30 Å.

All molecular dynamic simulations (MDS) were done using the software GROMACS-2021.1 [37], with all-atom CHARMM 36 force field [38], selecting a periodically corrected cubic box with a minimum distance of 1 nm. Next, the system was solvated with transferable intermolecular potential water model 3P (TIP3P), neutralized by the addition of $Na^+$ and $Cl^-$ ions, and 100,000 energy minimization steps were achieved using the steepest descent algorithm to eliminate initial steric shocks. The system was equilibrated for 500 and 2,500 ps at 310 K and 1 bar pressure in the NVT and NPT matrices, respectively and the productions were conducted during 50 ns long and coordinates were saved every 10 ps. All procedures were reached using the Leap-frog algorithm and Berendsen coupling to control pressure and temperature [39]. The Particle Mesh Ewald (PME) algorithm was used to analyze the long-range electrostatic interactions [40] and LINCS algorithm implementation was used to regulate the covalent bonds [41].

*Binding free energy calculation and Toxicological predictions*

To complement the molecular docking and MDS analyses were performed free energy calculations among 3TM0 and the selected ligands on a single trajectory based on the MMPBSA method [42], using the gmx-mmpbsa 1.5.4 software [43]. To perform the calculations were extracted the MDS results from all 50 ns of the runs, which were the equivalent of 1,000 snapshots for each simulation. The parameters that were used to calculate the binding free energies were inp=1, istrng=0.15, and indi=2, the other parameters were kept according to the software recommendations.

The profile of hepatotoxicity, carcinogenic, immunotoxicity, mutagenicity, and cytotoxicity were analyzed by using the ProTox-II web server [44].

*Visualizations of molecular docking and molecular dynamics results*

The 2D interaction diagrams and 3D protein-ligand interactions were generated with the software Discovery Studio Visualizer-2021. MDS analyses were visualized with GROMACS scripts in conjunction with Python scripts using the NumPy, Pandas, Matplotlib, Seaborn and Pytraj libraries. The RMSD, RMSF and Rg representations were generated from the alpha-carbon of the protein in the presence or absence of the ligands, while the H-bonds were generated from the protein and ligands information.

## 3. Results

*Virtual screening analyses of natural products on the nucleotide-binding pocket of EfAPH(3')-IIIa*

In the present work, the parameters used in the virtual screening with 3Q2J were the same described previously [19], allowing efficient re-docking of the co-crystallized ligand, CKI-7, in the nucleotide-binding pocket of the enzyme. On the other hand, for the analyses with the 2BKK and 3TM0 crystals and their respective co-crystals, ADP and ANP, the re-docking analyses were conducted. As shown in Fig. 1A and B, the re-docking results demonstrate values of 2.7 and 1.9, respectively for 2BKK-ADP and 3TM0-ANP. These results are due to the number of rotatable bonds in the co-crystals, as well as due to the structural resolution of the crystal complexes, reinforcing the importance of the selection of the ensemble docking approach.

The results of ensemble docking-based virtual screening demonstrated that the 3,092 natural products had binding affinities ranging from -11.1 to -3.8 kcal/mol (Supplementary Table 1, 2 and 3, respectively for 2BKK,3Q2J and 3TM0 crystals). The Pearson

Preprints (www.preprints.org) | NOT PEER-REVIEWED | Posted: 8 November 2022 doi:10.20944/preprints202211.0132.v1

correlation between the results of the three crystals was high, indicating similar affinity values of each ligand in the different crystals, with values above 0.9 for all comparative cases, Fig. 1C.

**Table 1.** Binding free energy calculation of ligands extracted from the single trajectory of MDS analyses of the three complexes.

| | Energy decomposition (Kcal/mol) ± standard deviation | | |
|---|---|---|---|
| | **BS-1** | **BS-2** | **BS-3** |
| **ΔE (Vdw)** | -27.9 ± 0.2 | -41.9 ± 1.8 | -39.5 ± 1.6 |
| **ΔE (Ele)** | -15.4 ± 1.6 | -11.9 ± 0.8 | -7.4 ± 0.1 |
| **ΔE (Polar, Solv)** | 25.9 ± 2.2 | 22.7 ± 0.4 | 18.2 ± 1.1 |
| **ΔE (non-Polar, Solv)** | -3.7 ± 0.3 | -4.3 ± 0.1 | -4.1 ± 0.1 |
| **ΔG (Total)** | -21.1 ± 2.9 | -35.3 ± 2.1 | -32.8 ± 2.2 |

**Table 2.** Comparative toxicological profile of BS-1, BS-2 and BS-3. Toxicological analyses were performed with the Pro-Tox II web server. Values in parentheses refer to probability.

| | Toxicological analyses | | |
|---|---|---|---|
| **Properties** | **BS-1** | **BS-2** | **BS-3** |
| **Hepatotoxicity** | Inactive (0.62) | Inactive (0.53) | **Active** (0.59) |
| **Carcinogenicity** | **Active** (053) | Inactive (0.51) | Inactive (0.58) |
| **Immunotoxicity** | Inactive (0.99) | Inactive (0.85) | Inactive (0.90) |
| **Mutagenicity** | Inactive (0.52) | Inactive (0.51) | Inactive (0.54) |
| **Cytotoxicity** | Inactive (0.58) | Inactive (0.70) | Inactive (0.77) |

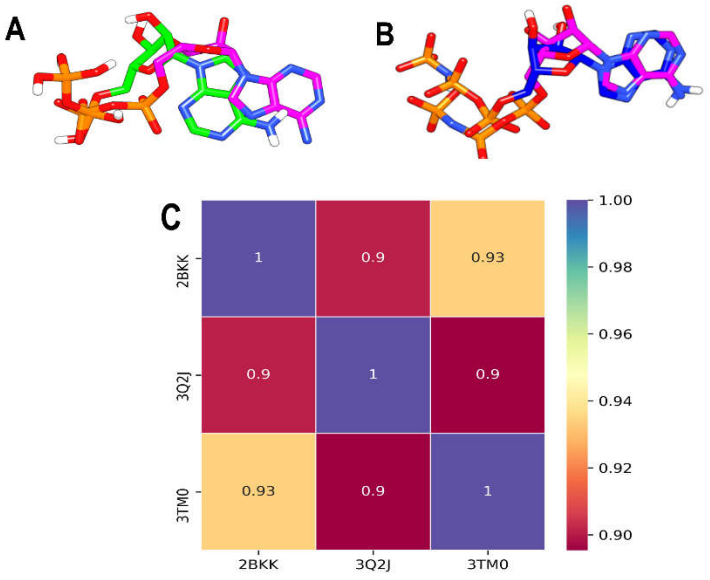


**Figure 1.** Redocking and Pearson correlation analysis. A) Redocking of ADP on the nucleotide-binding pocket of 2BKK. B) Redocking of ANP on the nucleotide-binding pocket of 3TM0. C) Pearson correlation of 3,092 natural products on the three different crystals 2BKK, 3Q2J and 3TM0.

To select the best ligands based on scoring performance in the three crystals, the rank-by-rank consensus strategy was used [45], Supplementary Table 4. The three best-ranked ligands were selected for further analysis. In descending order of best-score are the molecules BS-1 (ZINC000000952700, 4-methyl-2-oxochromen-7-yl) (2R)-2-(1,3-dioxoisoindol-2-yl)-3-phenylpropanoate, Fig. 2A), BS-2 (ZINC000014793040, N-(5-acetamido-2-methoxyphenyl)-3-methyl-4-oxo-2-phenylchromene-8-carboxamide, Fig. 2B) and, BS-3

Preprints (www.preprints.org) | NOT PEER-REVIEWED | Posted: 8 November 2022 doi:10.20944/preprints202211.0132.v1

(ZINC000015498603, N-(4-carbamoylphenyl)-2-pyridin-2-ylquinoline-4-carboxamide, Fig 2C). To perform MDS analyses the three best ligand poses obtained with the crystal 3TM0 were selected, since these showed the highest affinity binding values.

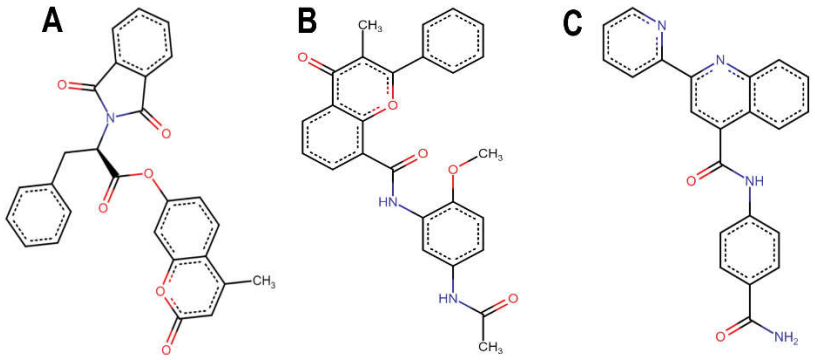


**Figure 2.** Structure of the best scored natural products. A) BS-1 (ZINC000000952700). B) BS-2 (ZINC000014793040). C) BS-3 (ZINC000015498603).

*Molecular dynamic simulations analyses of the complexes*

MDS analyses were conducted to better understand the stability, and interactions of the complexes formed by 3TM0 and the three best-scored ligands in the natural products database. The first analysis was the RMSD to determine the stability of the complexes. The complexes 3TM0-BS-1 and 3TM0-BS-3, despite scoring well in the rank-by-rank results, showed the largest fluctuations among the complexes analyzed. The RMSD values for both complexes increased from the beginning of the run, however, the ligands did not completely exit the nucleotide-binding pocket. The average RMSD value of 3TM0-BS-1 was 0.45 nm, while 3TM0-BS-3 obtained an average value of 0.43 nm. The 3TM0-BS-2 complex obtained fluctuations very similar to those obtained with the apo-3TM0 form (average RMSD of 0.20 nm), with an average RMSD value of 0.21 nm, Fig. 3A. From this information, it is observed that the BS-2 ligand was the most efficient in stabilizing 3TM0 during the simulation run.

The fluctuation results per amino acid residue show greater flexibility in the catalytic amino acids in the loop region of the nucleotide-binding (amino acids 23-29) and aminoglycoside-binding (amino acids 157-162) pockets. Fluctuations in the latter pocket will not be the focus of this study, so it will not be analyzed. The complexes 3TM0-BS-1, 3TM0-BS-2 and 3TM0-BS-3 showed a maximum fluctuation of 0.27, 0.31 and 0.28 respectively in the residues corresponding to the loop containing the catalytic amino acids, Fig. 3B. And it can be observed that the residues MET26 and SER27 of all complexes, which play a key role in enzyme catalysis [46], have smaller fluctuations in comparison with the apo-3TM0 form, which show RMSF of 0.53 nm. These results indicate that the interaction with the ligands stabilizes the enzyme.

The next results, of the Rg profiles, allowed the analysis of the compactness of each of the systems over the run time. All the complexes, as well as the apo-3TM0 form, showed very similar compactness values, on average the values were 0.93 nm. Considering the maximum values for each complex was observed that 3TM0-BS-1, 3TM0-BS-2 and 3TM0-BS-3 show respectively 1.96, 1.97 and 1.94 nm (Fig. 3C). The compactness profile of all complexes over the run time corroborate the RMSD and RMSF results that the ligands stabilize the enzyme.

Preprints (www.preprints.org) | NOT PEER-REVIEWED | Posted: 8 November 2022 doi:10.20944/preprints202211.0132.v1

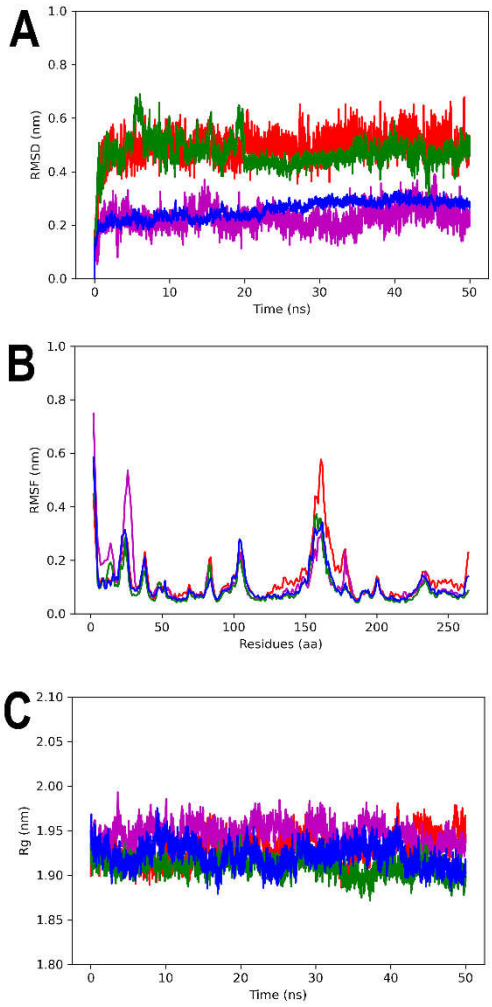


**Figure 3.** RMSD, RMSF and Rg analyses of 3TM0 and best-scored ligands BS-1, BS-2 and BS-3. A) RMSD values. B) RMSF values. C) Rg values. The colors red, magenta, green and blue represent respectively the complexes 3TM0-BS-1, 3TM0-BS-2, 3TM0-BS-3 and apo-3TM0.

Regarding hydrogen bonds over the run time, it can be seen that all three complexes were able to form these interactions. The complexes 3TM0-BS-1 and 3TM0-BS-2 obtained maximum values of five Fig. 4A and four Fig. 4B hydrogen bonds, but these were less constant compared to the 3TM0-BS-3 complex. The complex with the highest number and constancy of hydrogen bond interactions was 3TM0-BS-3, with a maximum of five interactions, two to three of which were maintained almost uninterruptedly during the run time, Fig. C.

Preprints (www.preprints.org) | NOT PEER-REVIEWED | Posted: 8 November 2022 doi:10.20944/preprints202211.0132.v1

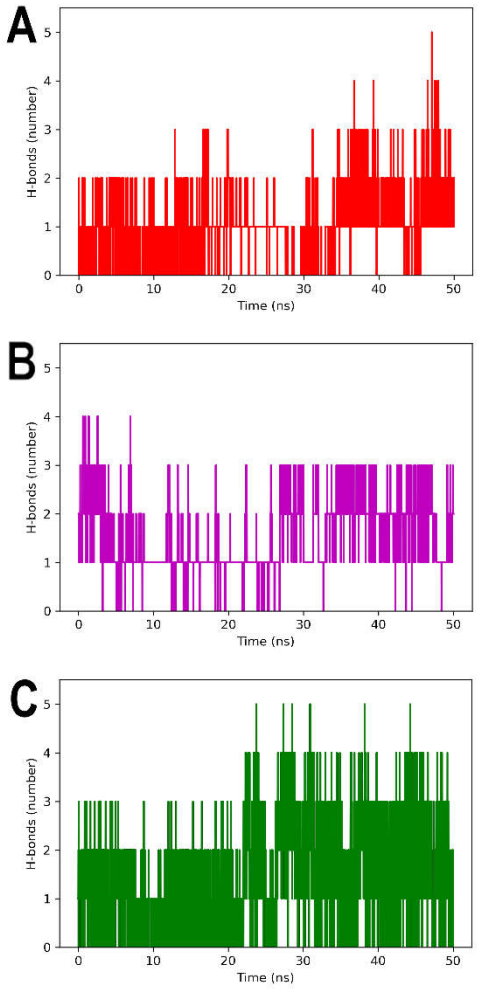


**Figure 4.** H-bonds number analyses of 3TMO complexed with A) BS-1, B) BS-2 and C) BS-3. The colors red, magenta and green represent respectively the complexes 3TM0-BS-1, 3TM0-BS-2 and 3TM0-BS-3.

*Binding Free energy calculation*

The binding free energy calculations for the three complexes show different results than those observed in the binding affinities obtained from virtual screening results. The total binding free energy calculation (ΔG, total) of -21.1, -35.3 and -32.8 kcal/mol were obtained for BS-1, BS-2 and BS-3, respectively, showing that the most favorable complex is 3TM0-BS-2. The results presented in Table 1 demonstrate that there is a higher contribution of Van der Waals interactions (ΔE, VdW of -27.9, -41.9 and -39.5 kcal/mol for BS-1, BS-2 and BS-3, respectively) to the total binding energy calculation compared to the contributions of electrostatic interactions (ΔE, ele of -15.4, -11.9 and -7.4 kcal/mol for BS-1, BS-2 and BS-3, respectively) and non-polar solvation energies (ΔE, non-Polar, Solv of -3.7, -4.3 and -4.1 kcal/mol for BS-1, BS-2 and BS-3, respectively). The polar solvation energies (ΔE, polar, Solv) that obtained values of 25.9, 22.7 and 18.2 kcal/mol, respectively for BS-1, BS-2 and BS-3, demonstrated that the formation of these interactions is not favorable for stabilizing the systems.

*Molecular docking analyses of best-scored ligands*

The molecular docking analysis allowed us to observe the profile of different types of interaction and also the position of each of the three ligands, acquired with the highest

Preprints (www.preprints.org) | NOT PEER-REVIEWED | Posted: 8 November 2022 doi:10.20944/preprints202211.0132.v1

energy poses for each of the studied complexes. The overlap analysis of these ligands on the aromatic surface of the nucleotide-binding pocket of the enzyme shows that the bicyclic aromatic backbones of each of the ligands are facing the TYR42 residue of the enzyme, forming pi-pi staked interactions (Fig. 5A). On the other hand, while BS-2 (Fig 5C). and BS-3 (Fig 5D). form hydrogen bonds (with MET26, SER27 and ASP208) through their acetamido and carbamoyl groups, respectively, BS1 forms no such bonds (Fig 5B). Overall, the results obtained from the molecular dynamics and energy calculation analyses are corroborated with the molecular docking results, where we observe the prevalence of Van der Waals interactions in these complexes.

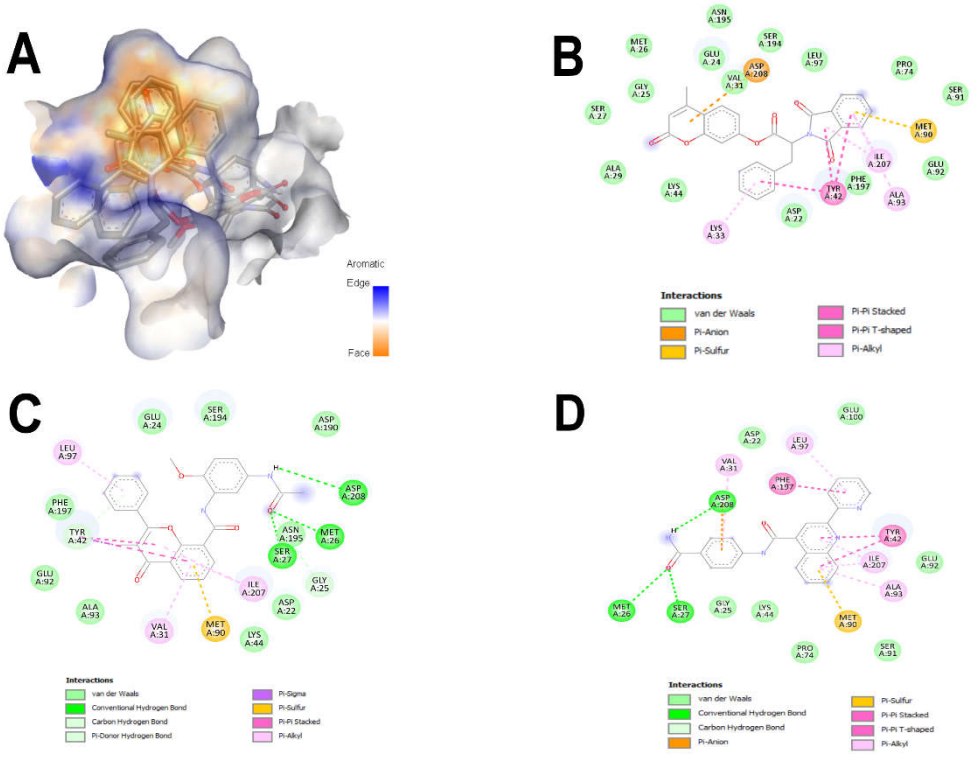


**Figure 5.** Overlap and 2D diagram of interactions of docking analysis between the best-scored natural products and 3TM0. A) Overlap of best-scored ligands on nucleotide binding pocket of EfAPH(3')-IIIa. B) 2D diagram interaction of BS-1 with 3TM0. C) 2D diagram interaction of BS-2 with 3TM0. D) 2D diagram interaction of BS-2 with 3TM0.

*Toxicological analysis*

To obtain preliminary information on the toxicological properties of these ligands, ProTox-II was used. The results reveal that BS-2 is the compound with the best profile due to the predicted absence of hepatotoxicity, carcinogenicity, immunotoxicity, mutagenicity, and cytotoxicity (Table 2). On the other hand, BS-1 and BS-3 show an active profile to act as carcinogenic and hepatotoxic, respectively.

## 4. Conclusion

In the current scenario, where a broad profile of resistance to available treatments is observed by some species such as *E. faecalis*, there is urgency in the discovery of new antibiotics or compounds that can act as adjuvants to them. In the approach taken in the present work, analyses were performed on 3,092 natural products obtained from the ZINC22 database to evaluate the nucleotide-binding pocket affinity of *Ef*APH(3')-IIIa using three different crystals. After filtering the best virtual screening scores using the rank-by-rank methodology, three ligands were selected: ZINC000000952700 (BS-1), ZINC000014793040 (BS-2) and ZINC000015498603 (BS-3). Of these, BS-2, a flavone

derivative demonstrated higher stability in MDS analyses, higher binding free energy predictions, and a better toxicological profiles. In addition, it was observed that BS-2 and BS-3 ligands were able to interact with key catalytic amino acids of the enzyme, such as MET26 and SER27, which make up the nucleotide-binding pocket. Taken together, these results show that the natural products studied in the present work may represent a promising scaffold for interacting with nucleotide-binding pocket of *Ef*APH(3')-IIIa.

**Conflicts of Interest:** The authors declare no competing financial interest.

## References


1. Hutchings, M.; Truman, A.; Wilkinson, B. Antibiotics: past, present and future. *Curr. Opin. Microbiol.* **2019**, *51*, 72–80, doi:10.1016/j.mib.2019.10.008.
2. Mohr, K.I. History of Antibiotics Research. In *How to Overcome the Antibiotic Crisis . Current Topics in Microbiology and Immunology*; 2016; Vol. 398, pp. 237–272.
3. World Health Organization *Antimicrobial resistance: global report on surveillance*; Geneva, 2014;
4. Fiore, E.; van Tyne, D.; Gilmore, M.S. Pathogenicity of enterococci. *Gram-Positive Pathog.* **2019**, 378–397, doi:10.1128/9781683670131.ch24.
5. Hollenbeck, B.L.; Rice, L.B. Intrinsic and acquired resistance mechanisms in enterococcus. *Virulence* **2012**, *3*, 421–569, doi:10.4161/viru.21282.
6. Jett, B.D.; Huycke, M.M.; Gilmore, M.S. Virulence of Enterococci. *Clin. Microbiol. Rev.* **1994**, *7*, 462–478, doi:10.1128/CMR.7.4.462.
7. Manoharan, H.; KV Lalitha, A.; Mariappan, S.; Sekar, U.; P. Venkataramana, G. Molecular Characterization of High-Level Aminoglycoside Resistance among Enterococcus Species. *J. Lab. Physicians* **2022**, doi:10.1055/s-0042-1742423.
8. Marino, A.; Munafò, A.; Zagami, A.; Ceccarelli, M.; Di Mauro, R.; Cantarella, G.; Bernardini, R.; Nunnari, G.; Cacopardo, B. Ampicillin plus ceftriaxone regimen against *Enterococcus faecalis* endocarditis: A literature review. *J. Clin. Med.* **2021**, *10*, doi:10.3390/jcm10194594.
9. Khan, A.; Miller, W.R.; Axell-House, D.; Munita, J.M.; Arias, C.A. Antimicrobial Susceptibility Testing for Enterococci. *J. Clin. Microbiol.* **2022**, *60*, e0084321, doi:10.1128/jcm.00843-21.
10. Kobayashi, N.; Mahbub Alam, M.; Nishimoto, Y.; Urasawa, S.; Uehara, N.; Watanabe, N. Distribution of aminoglycoside resistance genes in recent clinical isolates of *Enterococcus faecalis*, *Enterococcus faecium* and *Enterococcus avium*. *Epidemiol. Infect.* **2001**, *126*, 197–204, doi:10.1017/S0950268801005271.
11. Becker, B.; Cooper, M.A. Aminoglycoside antibiotics in the 21st century. *ACS Chem. Biol.* **2013**, *8*, 105–115, doi:10.1021/cb3005116.
12. Miller, W.R.; Munita, J.M.; Arias, C.A. Mechanisms of antibiotic resistance in enterococci. *Expert Rev. Anti. Infect. Ther.* **2014**, *12*, 1221–1236, doi:10.1586/14787210.2014.956092.
13. Krause, K.M.; Serio, A.W.; Kane, T.R.; Connolly, L.E. Aminoglycosides : An Overview. *Cold Spring Harb. Lab. Press* **2016**, *6*, 1–18, doi:10.1101/cshperspect.a027029.
14. Vakulenko, S.B.; Mobashery, S. Versatility of aminoglycosides and prospects for their future. *Clin. Microbiol. Rev.* **2003**, *16*, 430–450, doi:10.1128/CMR.16.3.430-450.2003.
15. Fong, D.H.; Berghuis, A.M. Substrate promiscuity of an aminoglycoside antibiotic resistance enzyme via target mimicry. *EMBO J.* **2002**, *21*, 2323–2331, doi:10.1093/emboj/21.10.2323.
16. Calderwood, S.A.; Wennersten, C.; Moellering, R.C.; Kunz, L.J.; Krogstad, D.J. Resistance to six aminoglycosidic aminocyclitol antibiotics among enterococci: prevalence, evolution, and relationship to synergism with penicillin. *Antimicrob. Agents Chemother.* **1977**, *12*, 401–405, doi:10.1128/AAC.12.3.401.
17. Feizabadi, M.M.; Maleknejad, P.; Asgharzadeh, A.; Asadi, S.; Shokrzadeh, L.; Sayadi, S. Prevalence of aminoglycoside-modifying enzymes genes among isolates of *Enterococcus faecalis* and *Enterococcus faecium* in Iran. *Microb. Drug Resist.* **2006**, *12*, 265–268, doi:10.1089/mdr.2006.12.265.
18. Padmasini, E.; Padmaraj, R.; Ramesh, S.S. High level aminoglycoside resistance and distribution of aminoglycoside resistant genes among clinical isolates of Enterococcus species in Chennai, India. *Sci. World J.* **2014**, *2014*, 1–6, doi:10.1155/2014/329157.
19. Carpio Arévalo, J.M.; Amorim, J.C. The Alpha-Naphthoflavone as a Novel Scaffold for the Design of Potential Inhibitors of APH(3')-IIIa of *Enterococcus faecalis*: An *In-Silico* Study. **2022**, doi:http://dx.doi.org/10.2139/ssrn.4206708.
20. Adriazola, I.O.; Amaral, A.E. Do; Amorim, J.C.; Correia, B.L.; Petkowicz, C.L.O.; Mercê, A.L.R.; Noleto, G.R. Macrophage activation and leishmanicidal activity by galactomannan and its oxovanadium (IV/V) complex *in vitro*. *J. Inorg. Biochem.* **2014**, *132*, 45–51, doi:10.1016/j.jinorgbio.2013.09.017.
21. Carpio Arévalo, J.M.; Feuser, P.E.; Rossi, G.R.; Trindade, E.S.; da Silva Córneo, E.; Machado-de-Ávila, R.A.; Sayer, C.; Cadena, S.M.S.C.; Noleto, G.R.; Martinez, G.R.; et al. Preparation and characterization of 4-nitrochalcone-folic acid-poly(methyl methacrylate) nanocapsules and cytotoxic activity on HeLa and NIH3T3 cells. *J. Drug Deliv. Sci. Technol.* **2019**, *54*, 101300, doi:10.1016/j.jddst.2019.101300.
22. Carpio Arévalo, J.M.; Amorim, J.C. An in-silico analysis reveals 7,7′-bializarin as a promising DNA gyrase B inhibitor on Gram-positive and Gram-negative bacteria. *Comput. Biol. Med.* **2021**, *135*, doi:10.1016/j.compbiomed.2021.104626.

23. Arévalo, J.M.C.; Amorim, J.C. Virtual screening, optimization and molecular dynamics analyses highlighting a pyrrolo[1,2-a]quinazoline derivative as a potential inhibitor of DNA gyrase B of *Mycobacterium tuberculosis*. *Sci. Rep.* **2022**, *12*, 1–13, doi:10.1038/s41598-022-08359-x.
24. Amorim, J.C.; Bermeo, A.E.C.; Urgilés, V.E.V.; León, M.R.M.; Carpio Arévalo, J.M. An *in silico* evaluation of anthraquinone derivatives as potential inhibitors of DNA gyrase B of *Mycobacterium tuberculosis*. **2022**, doi:https://doi.org/10.1101/2022.10.01.510436.
25. Butler, M.S.; Buss, A.D. Natural products - The future scaffolds for novel antibiotics? *Biochem. Pharmacol.* **2006**, *71*, 919–929, doi:10.1016/j.bcp.2005.10.012.
26. Tingle, B.I.; Tang, K.G.; Castanon, J.M.; Gutierrez, J.J.; Dandarchuluun, C.; Moroz, Y.S.; Irwin, J.J. ZINC-22 - A Free Multi-Billion-Scale Database of Tangible Compounds for Ligand Discovery. **2022**.
27. Irwin, J.J.; Tang, K.G.; Young, J.; Dandarchuluun, C.; Wong, B.R.; Khurelbaatar, M.; Moroz, Y.S.; Mayfield, J.; Sayle, R.A. ZINC20 - A Free Ultralarge-Scale Chemical Database for Ligand Discovery. *J. Chem. Inf. Model.* **2020**, *60*, 6065–6073, doi:10.1021/acs.jcim.0c00675.
28. Sander, T.; Freyss, J.; Von Korff, M.; Rufener, C. DataWarrior: An open-source program for chemistry aware data visualization and analysis. *J. Chem. Inf. Model.* **2015**, *55*, 460–473, doi:10.1021/ci500588j.
29. Halgren, T.A. Merck Molecular Force Field. I. Basis, Form, Scope, Parameterization, and Performance of MMFF94. *J. Comput. Chem.* **2000**, *17*, 520–552, doi:doi.org/10.1002/(SICI)1096-987X(199604)17:5/6<490::AID-JCC1>3.0.CO;2-P.
30. O'Boyle, N.M.; Banck, M.; James, C.A.; Morley, C.; Vandermeersch, T.; Hutchison, G.R. Open Babel: An open chemical toolbox. *J. Cheminform.* **2011**, *3*, 1–14.
31. Kohl, A.; Amstutz, P.; Parizek, P.; Binz, H.K.; Briand, C.; Capitani, G.; Forrer, P.; Plückthun, A.; Grütter, M.G. Allosteric inhibition of aminoglycoside phosphotransferase by a designed ankyrin repeat protein. *Structure* **2005**, *13*, 1131–1141, doi:10.1016/j.str.2005.04.020.
32. Fong, D.H.; Xiong, B.; Hwang, J.; Berghuis, A.M. Crystal structures of two aminoglycoside kinases bound with a Eukaryotic protein kinase inhibitor. *PLoS One* **2011**, *6*, 1–7, doi:10.1371/journal.pone.0019589.
33. Fong, D.H.; Berghuis, A.M. Structural Basis of APH(3′)-IIIa-Mediated Resistance to N1-Substituted Aminoglycoside Antibiotics. *Antimicrob. Agents Chemother.* **2009**, *53*, 3049–3055.
34. Pettersen, E.F.; Goddard, T.D.; Huang, C.C.; Couch, G.S.; Greenblatt, D.M.; Meng, E.C.; Ferrin, T.E. UCSF Chimera - A visualization system for exploratory research and analysis. *J. Comput. Chem.* **2004**, *25*, 1605–1612, doi:10.1002/jcc.20084.
35. Morris, G.M.; Huey, R.; William Lindstrom; Sanner, M.F.; Belew, R.K.; Goodsell, D.S.; Olson, A.J. AutoDock4 and AutoDockTools4: Automated Docking with Selective Receptor Flexibility. *J. Comput. Chem.* **2009**, *30*, 2785–2791, doi:10.1002/jcc.
36. Trott, O.; Olson, A.J. Software News and Updates AutoDock Vina: Improving the Speed and Accuracy of Docking with a New Scoring Function, Efficient Optimization, and Multithreading. *J. Comput. Chem.* **2012**, *32*, 174–182, doi:10.1002/jcc.
37. Van Der Spoel, D.; Lindahl, E.; Hess, B.; Groenhof, G.; Mark, A.E.; Berendsen, H.J.C. GROMACS: Fast, flexible, and free. *J. Comput. Chem.* **2005**, *26*, 1701–1718, doi:10.1002/jcc.20291.
38. Best, R.B.; Zhu, X.; Shim, J.; Lopes, P.E.M.; Mittal, J.; Feig, M.; MacKerell, A.D. Optimization of the additive CHARMM all-atom protein force field targeting improved sampling of the backbone φ, ψ and side-chain χ1 and χ2 Dihedral Angles. *J. Chem. Theory Comput.* **2012**, *8*, 3257–3273, doi:10.1021/ct300400x.
39. Berendsen, H.J.C.; Postma, J.P.M.; Van Gunsteren, W.F.; Dinola, A.; Haak, J.R. Molecular dynamics with coupling to an external bath. *J. Chem. Phys.* **1984**, *81*, 3684–3690, doi:10.1063/1.448118.
40. Ewald, P.P. Die Berechnung optischer und elektrostatischer Gitterpotentiale. *Ann. Phys.* **1921**, *369*, 253–287, doi:10.1002/andp.19213690304.
41. Hess, B.; Bekker, H.; Berendsen, H.J.C.; Fraaije, J.G.E.M. LINCS: A Linear Constraint Solver for molecular simulations. *J. Comput. Chem.* **1997**, *18*, 1463–1472, doi:10.1002/(SICI)1096-987X(199709)18:12<1463::AID-JCC4>3.0.CO;2-H.
42. Kollman, P.A.; Massova, I.; Reyes, C.; Kuhn, B.; Huo, S.; Chong, L.; Lee, M.; Lee, T.; Duan, Y.; Wang, W.; et al. Calculating structures and free energies of complex molecules: Combining molecular mechanics and continuum models. *Acc. Chem. Res.* **2000**, *33*, 889–897, doi:10.1021/ar000033j.
43. Valdés-Tresanco, M.S.; Valdés-Tresanco, M.E.; Valiente, P.A.; Moreno, E. Gmx_MMPBSA: A New Tool to Perform End-State Free Energy Calculations with GROMACS. *J. Chem. Theory Comput.* **2021**, *17*, 6281–6291, doi:10.1021/acs.jctc.1c00645.
44. Banerjee, P.; Eckert, A.O.; Schrey, A.K.; Preissner, R. ProTox-II: A webserver for the prediction of toxicity of chemicals. *Nucleic Acids Res.* **2018**, *46*, W257–W263, doi:10.1093/nar/gky318.
45. Wang, R.; Wang, S. How Does Consensus Scoring Work for Virtual Library Screening? An Idealized Computer Experiment. *J. Chem. Inf. Comput. Sci.* **2001**, *41*, 1422–1426, doi:10.1021/ci010025x.
46. Thompson, P.R.; Boehr, D.D.; Berghuis, A.M.; Wright, G.D. Mechanism of aminoglycoside antibiotic kinase APH(3′)-IIIa: Role of the nucleotide positioning loop. *Biochemistry* **2002**, *41*, 7001–7007, doi:10.1021/bi0256680.